HHS Public Access

Author manuscript

*Virology*. Author manuscript; available in PMC 2019 October 01.

Published in final edited form as:

*Virology*. 2018 October ; 523: 110–120. doi:10.1016/j.virol.2018.08.003.

# The C-terminus of varicella-zoster virus glycoprotein M contains trafficking motifs that mediate skin virulence in the SCID-human model of VZV pathogenesis

**Zerboni Leigh**[1,*], **Sung Phillip**[1], **Sommer Marvin**[1], and **Arvin Ann**[1,2]

[1]Departments of Pediatrics, Stanford University School of Medicine, Stanford, CA

[2]Departments of Microbiology & Immunology, Stanford University School of Medicine, Stanford, CA

## Abstract

Knowledge about the function of varicella-zoster virus glycoprotein M is limited; the requirement of gM for skin and neural tropism are unknown. VZV gM contains two predicted YXXΦ trafficking motifs and a dileucine motif in the carboxyl-terminus. We constructed a recombinant VZV with gM truncated from the first YXXΦ and five additional viruses with YXXΦ tyrosine substitutions, alone and in combination with dileucine substitution. All recombinant viruses grew to high titer but mutation of the membrane-proximal YXXΦ motif reduced plaque size in cultured cells and altered gM localization. C-terminus truncation had a pronounced effect on virion morphogenesis and plaque size, but not on overall replication kinetics in vitro. Mutation of gM trafficking motifs and truncation attenuated replication in human skin xenografts in vivo; gM truncation did not alter neurotropism. Our results demonstrate that the gM C-terminus is dispensable for virus replication in cultured cells but is important for skin pathogenesis.

### Keywords

varicella-zoster virus; herpes; SCIDhu; glycoprotein M

## INTRODUCTION

Varicella-zoster virus (VZV) is the human alphaherpesvirus that causes varicella upon primary infection in susceptible persons and establishes a lifelong latent infection in sensory neurons from which it may reactivate causing herpes zoster (1). The VZV genome contains open reading frames (ORFs) encoding for at least nine glycoproteins, including glycoprotein (g)M (2). Herpesviral gM species are highly conserved. Orthologous gM species are generally required for beta- and gammaherpesvirus replication but are dispensable to most

[*]Corresponding author: Leigh Zerboni, MS, Stanford University School of Medicine, 300 Pasteur Dr., Stanford, CA 94305; Tel.: 650-498-6227. zerboni@stanford.edu.

alphaherpesviruses (3–6). Several studies indicate that gM species are modulators of virally induced cell fusion, although the mechanism is unclear (4–6). Interestingly, pseudorabies virus and bovine herpes virus gM orthologs inhibit fusion induced by unrelated viral proteins, such as the bovine respiratory syncytial virus F protein (5, 6). VZV gM is a multipass integral membrane protein that is incorporated into the virion envelope; it is not essential for VZV replication in cultured cells (7). The phenotypes for a VZV gM truncation mutant and a maturation defective mutant include small plaque size, reduced syncytia formation, and reduced viral titers *in vitro* (7, 8).

Intracellular trafficking motifs are found on the carboxyl-terminal domains of many cellular and viral transmembrane proteins. These protein regulatory sequences are usually encoded as 4 to 7 contiguous amino acids (aa) and are recognized by host adapter proteins (AP) of the cellular endocytic and sorting pathways. The aa sequence YXXΦ where X is any aa and phi(Φ)is any bulky hydrophobic aa, is a dual internalization and trafficking specific signal that facilitates adapter protein-mediated internalization from the cell surface to a specific intracellular site through interaction with the respective mu(μ) subunit of the clathrin complex (9–11). In this tetrapeptide sequence, the tyrosine residue is critical for the signal (12). Acidic dileucine clusters, typically DXXLL and [D/E]XXXL[LVI], target membrane proteins from the *trans* Golgi network (TGN) to lysosomal/endosomal compartments through interaction with AP complexes (12)(13).

Most alphaherpesviral glycoproteins have YXXΦ and/or dileucine trafficking motifs, including VZV gE, gI, gB and gH (14–16) and all herpesviral gM orthologs (17, 18). These sequences are presumed to mediate a physical interaction between membrane-localized viral glycoproteins with the clathrin-associated AP-2 complex, initiating internalization and redirection to the TGN, the site of virion assembly in the cytosol (16, 19). It has also been proposed that some gM YXXΦ sequences drive internalization of other herpesviral envelope proteins, such as HSV-1 gE (20, 21). The cytoplasmic tail of VZV gE contains two YXXΦ sequences; mutation of the membrane-proximal YAGL sequence is detrimental for replication (22). The cytoplasmic tail of VZV gB also contains two YXXΦ sequences and a dileucine motif; the membrane-proximal YSRV aa sequence is primarily responsible for gB endocytosis but is dispensable for replication (15). A dileucine motif in the cytoplasmic tail of VZV gI mediates endocytosis (16); endocytosis of VZV gH is mediated by a YNKI aa sequence in the cytoplasmic tail (14).

Despite the high degree of conservation, mutation or deletion of alphaherpesviral endocytosis trafficking sequences is seldom detrimental to virus replication in cultured cells (17, 18). Some VZV mutants with altered glycoprotein trafficking exhibit defects in viral assembly, but are replication competent (14–16). In addition to their role in directing membrane protein internalization and intracellular relocalization, it has been proposed that herpesviral glycoprotein trafficking sequences may be required for directional movement of glycoproteins to epithelial cell junctions during skin infection *in vivo* and/or anterograde transport of virus envelope proteins in neuronal axons (23, 24). Of note, mutation of the VZV gE YYRV sequence accelerates growth *in vitro*, attenuates replication in skin xenografts (22), and is dispensable for neurovirulence (25). These disparate phenotypes illustrate the importance of examining YXXΦ sequence function *in vivo*. The aim of our

study was to examine the effect of combinatorial mutations of different gM C-terminal endocytosis motifs on VZV virulence in cultured cells as well as differentiated human skin and neural xenografts *in vivo*.

## RESULTS AND DISCUSSION

### Generation of recombinant gM viruses with mutations in putative trafficking motifs located in the carboxyl-terminal domain.

VZV gM is predicted to have a 76 aa intracellular C-terminus after the final transmembrane domain (TMD) at aa360 (26). We performed a linear motif scan of the gM cytoplasmic tail (Eukaryotic Linear Motif resource at http://elm.eu.org) (11) and identified two YXXΦ motifs (YGAV, aa 373–376 and YGYV, aa 407–410) and a single dileucine motif (REDELL, aa 421 to 426) (Fig. 1A).

We constructed recombinant VZV strains with mutations in these putative gM trafficking motifs using the VZV five cosmid system, which consists of five overlapping fragments of genomic vaccine (Oka strain) DNA cloned into SuperCos-1 cosmid vectors (27) (Fig. 1B). ORF50 encodes VZV gM on the reverse strand at nucleotides (nt) 20198–18891 of the 28506 basepair (bp) pvAvr10 cosmid. As described in **Methods**, mutagenic PCR primers for a pvAvr10 subclone were designed for Y to A substitution in the membrane-proximal gM YXXΦ motif, Y to S substitution in the second gM YXXΦ motif, LL to HV substitution in the gM dileucine motif, and stop codon insertion to generate a gM truncated at the C-terminus. When co-transfected with intact cosmids, five recombinant viruses were generated with individual or combined mutations in the YXXΦ and LL motifs, and a C-terminal stop codon mutant was generated lacking the last 59 amino acids of VZV gM (Fig. 1A). Virus was recovered from cosmids sets within 5–7 days post transfection for parental recombinant vaccine Oka (rVOka) and all mutagenic clones except gM C-term stop, which was recovered at 9 days post transfection. The resulting viruses were named gM Y373A, gM LL425HV, gM Y373A+LL425HV, gM double YXXΦ, gM triple mutant and gM C-term stop (Fig. 1A); mutations were verified by PCR and sequencing.

### Replication kinetics of VZV gM C-terminal mutants.

Viral replication kinetics of the gM C-terminal mutant viruses were assessed by growth curves in melanoma (MeWo) cells over 6 days (Fig. 2**)**. For all mutants and recombinant rVOka, viral titers peaked at day four. All mutants grew equally well as rVOka through day five, by which point many viruses had exhausted the supply of uninfected cells in wells and titers began to decrease. All titer plates were fixed and stained using anti-VZV antibody and FastRed substrate to facilitate counting accuracy of mutants with small plaques. Representative immunostaining of viral plaques at 3 days after infection are shown in Fig. 2B (rVOka) and Fig. 2C (gM C-term stop).

### VZV gene expression in gM mutant viruses.

At 24 hours after infection, accumulation of VZV gM protein in infected cell lysates was examined by immunoblot using a mono-specific rabbit anti-VZV gM antibody (Fig. 3). The mono-specific antibody recognizes the terminal 14 aa of gM; this epitope is not expressed in

gM C-term stop mutant (Fig. 3A, lane 5). Absence of any anti-gM reactivity in the gM C-term stop mutant demonstrates that the stop codon insertions were sufficient to truncate gM without any readthrough. Expression of immediate early (IE) 63 protein (Fig. 3C) and glycoprotein E (Fig. 3D) were also examined; all were expressed with no differences noted relative to expression in rVOka-infected cells. Expression of cellular tubulin was assessed as a loading control (Fig. 3E). This result demonstrates that mutation of the YXXΦ motifs alone or in combination with the dileucine motif does not impair synthesis of the ORF50 gene product, or expression of representative proteins from other kinetic classes.

### The C-terminus of VZV gM facilitates cell-cell spread of virus in cultured cells.

Plaque size is a phenotypic marker used to evaluate the capacity of a virus to spread and produce cytopathic changes in localized foci. As VZV is a cell-associated virus, this property is critical as infection can only spread from one infected cell to an adjacent uninfected cell, leading to the formation of multinucleated polykaryocytes and syncytia. Endocytosis of viral glycoproteins, in particular fusion proteins that facilitate entry (gH, gB), are presumed to regulate virus-induced cell-cell fusion (28–30).

We assessed the capacity for VZV C-terminal mutants to spread from cell to cell, producing viral plaques, by measuring the Feret diameter of plaques three days after infection. Plaques were measured after immunohistochemical staining, using FastRed precipitate as the boundary indicator (Fig. 4). Viral plaques from gM LL425HV mutants were equivalent in size to rVOka, indicating that the dileucine motif at aa425 does not contribute to cell-cell spread *in vitro*. All VZV gM mutants that contain the Y373A substitution produced smaller plaques when compared with rVOka, indicating that this motif is required for efficient cell-cell spread *in vitro*. Plaques formed in cells infected with the gM double YXXΦ were similar in size to gM Y373A plaques, demonstrating that mutation of the second YXXΦ motif does not augment the small plaque phenotype of gM Y373A. In addition, the reduction in plaque size was not augmented by mutation of the dileucine motif in combination with both YXXΦ motifs. However, removal of the terminal 59 aa of VZV gM (gM C-term stop) significantly reduced plaque size compared with rVOka and gM Y373A. This result indicates that the YXXΦ motif at aa 373–376 is important for efficient cell-cell spread *in vitro* and that other determinants of cell-cell spread are contained within the C-terminus of VZV gM.

### Intracellular localization of VZV gM in cultured cells is dependent on YXXΦ sequences.

YXXΦ sequences are presumed to facilitate interaction between membrane-localized viral glycoproteins and cellular clathrin-associated AP complexes, to relocate mature glycoproteins to sites of virion assembly in the cytosol (16, 19). Nascent VZV capsids acquire tegument proteins and the glycoprotein-containing envelope at perinuclear cisternae of the TGN, and then move to the cell surface in TGN-derived vesicles (18, 19, 31). In cultured cells, gM primarily co-localizes with cell markers for the TGN (7). We evaluated the cellular localization of VZV gM by immunofluorescence staining of fibroblasts infected with rVOka (Fig. 5A), gM double YXXΦ (Fig. 5B) and gM triple mutant (Fig. 5C) at 48 hours after infection. VZV plaques were stained using a mouse anti-VZV gE (Fig. 5, red signal). VZV gE has a distinct Golgi-compartment distribution and an intense signal on

infected cell membranes (32). VZV gM was identified using rabbit gM-antibody (Fig. 5, green signal).

In rVOka-infected cells, gM was primarily observed in the perinuclear region of infected cells at the plaque periphery (Fig. 5A, white box), and co-localized with VZV gE. Some dim staining along host cell membranes at the plaque center, forming a large syncytium of fused cells, was also observed (Fig. 5A, white arrow). In the smaller plaques induced by the gM double YXXΦ and gM triple mutant viruses, multinucleated syncytia were observed but were not as large and contained fewer accumulated nuclei than in rVOka-infected cells (Fig. 5B and5C, white arrows). As in rVOka-infected cells, gM expression was observed to be perinuclear in infected cells at the plaque periphery; in addition, many cells also contained punctate gM expression within the cellular cytoplasm (Fig. 5B and5C, white boxes and inset panels). No differences were apparent when comparing the gM double YXXΦ mutant and the gM triple mutant, indicating that this punctate gM expression phenotype can be attributed to mutation of the YXXΦ motifs. The accumulation of punctate gM in the absence of gM YXXΦ signals indicates that the tyrosine residues at aa 373 and aa 407 are required for the complex array of routing and trafficking decisions directed by these motifs.

### VZV lacking the C-terminus of gM is impaired in virion morphogenesis.

VZV glycoproteins play a critical role in VZ virion morphogenesis, which requires specific protein-protein interaction mediated by the cytoplasmic tail of membrane viral glycoproteins, as illustrated by mutagenesis of VZV gE and gI (22, 33). Virion particle formation and viral egress was assessed by transmission electron microscopy (TEM) of melanoma cells infected with rVOka (Fig. 6A), gM Y373A (Fig. 6B), gM LL425HV (Fig. 6C), gM Y373A+LL425HV (Fig. 6D) and gM C-term stop (Fig. 6E–6F) at 3 days after infection. In rOka-infected cells, cytoplasmic VZ virions were abundant and readily observed within vesicles; some small vesicles contained one or more particles, some larger vesicles contained multiple pleomorphic appearing particles (Fig. 6A-D, white arrows). These post-Golgi compartment vesicles contain nascent virions and are presumed to traffic and fuse with the outer cell membrane (34). Similar vesicles were observed in all gM mutants with altered YXXΦ and LL motifs; dense VZ particles were readily observed on the outer cell membranes of cells infected with these gM mutants. This observation indicates that lack of these sorting motifs does not impair virion particle assembly or egress to the cell surface.

In contrast, in gM C-term stop infected cells, these vesicles were only rarely observed and did not contain enveloped particles. Electron dense particles similar in size to capsids accumulated in Golgi areas; these particles lacked any associated tegument or envelope (Fig. 6E, white arrow). Viral particles were rarely observed on the plasma membranes of gM C-term stop infected cells (Fig. 6F). The accumulation of defective and immature VZ capsids that we observed by TEM in cultured cells infected with gM C-term stop indicates that the cytoplasmic tail of gM is required for virion maturation and incorporation into the viral envelope, but this dependency does not require gM YXXΦ and dileucine trafficking motifs.

### VZV gM facilitates replication in differentiated human skin xenografts in vivo.

We have previously observed that glycoprotein trafficking and signaling motifs function in tissue-specific tropism of VZV (22, 25). Therefore, we utilized the SCIDhu model to determine if nonlethal mutation of gM trafficking motifs can alter viral replication and virulence within intact differentiated human skin and neural tissue. In two separate experiments, differentiated human skin xenografts maintained in SCIDhu mice were inoculated with equivalent PFU/ml of VZV gM mutant viruses. Replication in skin tissues was assessed at 11 and 21 days post inoculation (Fig. 7A). In the first skin experiment, the gM Y373A, gM LL425HV and gM Y373A+LL425HV mutants were evaluated and compared with rVOka. All three gM mutants grew equally well compared with rVOka at the early timepoint, with the expected increase in viral titers as infection progressed and overall infectious virus recovery in 80–100% of implants for each virus. Of note, the gM LL425HV mutant exhibited higher viral titers from homogenized skin tissue at 21 days after infection, but the level of increase was not significant when compared with rVOka or gM Y373A.

In the second skin experiment, the gM double YXXΦ, gM triple mutant and gM C-term stop mutant were evaluated. All gM mutants exhibited the expected increase in viral titer as infection progressed. Despite the reduced plaque size and altered gM localization exhibited *in vitro*, the gM double YXXΦ mutant grew to an equivalent titer as rVOka by 21 days after infection. However, only 3 of 6 homogenized skin tissues contained infectious virus at the early timepoint. Mutation of both YXXΦ motifs in combination with dileucine substitution (gM triple mutant) also resulted in poor recovery of infectious virus at the early timepoint (2 of 5 tissues, 40%), and significantly reduced viral titers in VZV+ tissues, but by day 21 replication in skin approached levels exhibited by rVOka. This indicates that these highly conserved endocytosis motifs are not strictly required for skin virulence, but mutation of these trafficking signals produces a delayed-growth phenotype. This also indicates that the dileucine motif, whose functionality could not be demonstrated *in vitro*, does contribute to skin virulence in synergy with the YXXΦ motifs.

Replication of the gM C-term stop mutant was significantly impaired in skin xenografts. At the early timepoint, viral titers were significantly lower when compared with rVOka and infectious virus was only recovered from 3 of 6 implants. This growth impairment continued through day 21, with significantly reduced viral titers and poor virus recovery. This result demonstrates that the C-terminus of VZV gM is a virulence determinant for replication in skin *in vivo.*

### VZV gM C-terminus facilitates VZV spread within differentiated human skin tissues.

To examine the extent of VZV spread and lesion formation induced by skin infection with gM trafficking mutants, we examined tissue sections from VZV-infected skin xenografts by immunostaining with a high potency rabbit anti-IE63. Representative images are shown in Fig. 8. Histological features of full thickness uninfected skin xenografts (Fig. 8A) include organized epidermal (E) and dermal (D) compartments separated at the basal lamina by the dermal-epidermal junction (Fig. 8A, arrows). The dermis is primarily comprised of dermal fibroblasts; epidermal keratinocytes are the product of stem cells at the basal lamina that

constantly renew, stratify and keratinize the layers above. Skin xenografts also contain epidermal appendages, such as hair follicles and glands projecting into the dermis.

In skin xenografts infected with rVOka-infected and examined at 21 days after infection (Fig. 8B), histopathology and IE63-reactivity was consistent with varicella lesions observed in biopsy specimens of varicella skin lesions, including the presence of degenerative ballooning cells and multinucleated polykaryons within an epithelial-localized debris field (35). These large suprabasal vesicles are thought to contain cell free infectious particles (36). As these lesions grow, the epidermis is often observed to separate at the spinous layer, a process called acantholysis (Fig. 8B, black arrow), which we observed in rVOka-infected skin lesions. We also observed that the basement membrane separating the epidermal and dermal compartments appeared thinned and discontinuous. Hair follicles and epidermal appendages displayed strong IE63-reactivity, indicating cell-cell spread to the dermal compartment (Fig. 8B, white arrow).

Lesion histopathology in xenografts infected with the gM triple mutant were similar to those produced by rVOka with respect to observations in the epidermal compartment. Intense IE63-immunoreactivity was observed in balloon cells and polykaryons within the suprabasal debris field; acantholysis was observed. In the dermal compartment, IE63-immunoreactivity was reduced, including within epidermal appendages, indicating a diminished capacity for cell-cell spread in skin (Fig. 8C). We typically observe that VZV mutants with small plaque size in culture are unable to spread efficiently through the dermal-epidermal junction into the papillary dermis in human skin xenografts (22, 37, 38). The delayed-growth phenotype and reduced dermal spread of the gM triple mutant demonstrates a role for gM YXXΦ and dileucine trafficking motifs in skin virulence.

Like the gM triple mutant, the gM C-term stop mutant also exhibited a small plaque phenotype in culture and skin viral titers were significantly reduced. Unexpectedly, the histological skin phenotype was different than both rVOka and the gM triple mutant. In skin sections from gM C-term stop infected xenografts, lesion size was very small in the suprabasal stratum, the cornified stratum remained intact and acantholysis was not observed. Despite the small lesion size, IE63-reactivity was intense within these small lesions, and spread through the dermal-epidermal compartment and to hair follicles was observed (Fig. 8D). This result suggests that in addition to trafficking motifs, the gM C-terminus contains regulatory sequences that facilitate suprabasal vesicle formation in skin.

## The VZV gM C-terminus is not required for formation of neuron-satellite cell complexes or satellite glial cell tropism.

Histological analysis of ganglia from patients with zoster at the time of death demonstrated that cell-cell spread resulting in polykaryon formation is also a characteristic of VZV neurotropism (39). VZV induces fusion between differentiated neurons and surrounding satellite cells during infection of dorsal root ganglia xenografts, presumably aided by the same viral glycoproteins that mediate cell-cell spread in skin (40, 41). Previously, we demonstrated that a gE mutant with defective TGN trafficking was replication competent in human DRG xenografts *in vivo*; whereas replication of a gI null mutant with impaired virion assembly and skin tropism, was severely restricted (25, 42). Therefore, we hypothesized that

the gM C-term stop mutant may be similarly restricted for replication and spread in human sensory ganglia using the SCIDhu DRG mouse model.

Human DRG engrafted under the murine renal capsule were inoculated with 1000 PFU/implant by direct injection and evaluated by immunostaining for VZV proteins at 21 days after infection, when peak levels of replication are expected. Immunoreactivity to anti-VZV antibody was observed in axons and neuronal cell bodies, as well as supportive satellite glial cells in DRG infected with rVOka (Fig. 8E) and the gM C-term stop mutant (Fig. 8F). Fusion of neuronal and satellite cell membranes, forming neuron-satellite cell complexes, was observed in rVOka- and gM C-term stop-infected neurons (Fig. 8F, white arrow). This result indicates that the C-terminus of VZV gM is not required for VZV replication in neurons and supportive satellite cells *in vivo*.

### Concluding remarks.

Our examination of the VZV gM carboxy-terminus demonstrates that tyrosine substitution within the membrane-proximal YXXΦ motif alone, or in combination with the second YXXΦ motif reduces plaque size but does not alter replication kinetics *in vitro*. The combined YXXΦ motifs at aa373–376 and aa407–410 contribute to gM perinuclear localization. Neither gM YXXΦ motifs are required for skin virulence *in vivo;* however, mutation of both in combination with the dileucine motif at aa425 attenuates replication and spread in skin. Further, we demonstrate that truncation of VZV gM at aa375 does not alter replication kinetics *in vitro* or neurotropism but severely restricts virion maturation and reduces plaque size in cultured cells. The cytoplasmic tail of VZV gM is a determinant of virulence in skin.

## MATERIALS AND METHODS

### Generation of recombinant gM mutant viruses.

Mutations in VZV gM at the native site were produced using the VZV five cosmid system, which has been previously described (27). Briefly, when co-transfected into a permissive cell line, the VZV genomic fragments (pvFsp4, pvSpe5, pvAfl30, pvAvr10 and pvSpe21) recombine producing a single clone of infectious recombinant VZV (Fig. 1B). Individual cosmids can be used for site-directed mutagenesis and then substituted for intact cosmids. To facilitate subcloning and PCR mutagenesis, a reverse-complement 7071 bp NheI – SalI fragment of pAvr10 spanning part of ORF47 to ORF51 was subcloned into the pET BLUE-2 vector (Novagen, San Diego, CA) and the resulting plasmid (pETAVR) was used to generate all VZV gM mutants. Prior to cosmid transfection, the native fragment in the pvAvr10 cosmid was replaced with the mutated NheI-SalI fragment. In all, six mutated pETVAVR fragments were generated. For mutagenesis of the first YXXΦ motif at aa 373–376, mutagenic PCR primers were designed to amplify two fragments, one of which extended from an upstream BamHI site to a newly created NarI site and which substituted alanine (A) for tyrosine (Y) in the YGAV motif. The second fragment extended from a newly created NarI site to a downstream SacI site. The BamHI-NarI and NarI-SacI fragments were ligated and replaced the original BamHI-SacI fragment in pETVAVR, generating the new plasmid pETVAVR_gM-Y373A. This NheI-SalI fragment from pETVAVR_gM-Y373A was isolated

and replaced the native fragment in the pvAvr10 cosmid creating the new mutagenic cosmid pvAvr10_gM- Y373A.

Using a similar strategy, PCR primers were designed for mutagenesis of the dileucine motif, replacing the leucine-leucine at aa 425–426 for histidine-valine. To generate the plasmid pETVAVR_gM-Y373A+LL425HV, the pETVAVR_gM-Y373A plasmid was digested with RsrII and SacI, and the 166 bp RsrII-SacI fragment was replaced with the RsrII-SacI fragment containing the HV substitution. Using both the pETVAVR_gM-Y373A and pETVAVR_gM Y373A+LL425HV plasmids as a template, PCR primers were designed to create a new BamH1 site and substituted a serine for tyrosine at aa 407, generating plasmids pETVAVR_gM-double YXXΦ and pETVAVR_gM-triple mutant. Truncation of gM in pETVAVR was accomplished by using primer pairs which replaced aa 376–378 and aa 381 with two in-frame stop codons and one frame-shifted stop signal and created a new NarI site. For all mutants, PCR products were gel purified and ligated into pCR4-TOPO cloning vector (Invitrogen, Carlsbad, CA) and amplification products were verified by sequence analysis using M13 reverse/forward primers.

Infectious recombinant VZV gM mutant viruses produced by cotransfection of pvFsp4, pvSpe5, pvAfl30, and pvSpe21 cosmids in combination with intact pvAvr10 or mutagenic pvAvr10 cosmid were passaged when monolayers were confluent and maintained until viral plaques were evident. The presence of the expected mutations and absence of any other mutations were verified by PCR amplification and sequencing of the ORF50 coding region. Viruses were propagated in human melanoma cells (MeWo cell line, ATCC HTB65) and primary human embryonic lung fibroblasts (HELF) cells for *in vivo* experiments (passage number <20). MeWo and fibroblast cells were maintained in Dulbecco's modified Eagle's medium (Life Technologies #12400–024) supplemented with 10% inactivated fetal calf serum, and 1X penicillin, streptomycin and glutamine.

### Replication kinetics and viral titrations.

To examine replication kinetics of gM mutant viruses, growth curve analysis was performed by adding 1000 PFU of each virus onto 6-well plates containing $1\times10^6$ Mewo cells/well. Replicate wells (two per virus) were harvested daily for six days and viral titrations were performed. Viral titrations for all experiments were done using $1.5\times10^5$ MeWo cells/well in 24-well plates. A 0.1 ml virus-cell suspension was serially diluted and titrated in triplicate wells. After 3 days in culture at 37˚ C in 5% $CO_2$, plates were fixed for 20 minutes in 4% paraformaldehyde, and rinsed with phosphate-buffered saline, pH 7.4 (PBS). Viral plaques were visualized by immunohistochemical staining using a mouse anti-VZV polyclonal serum (C05108MA; Meridian Life Science). Fixed plates were air dried and blocked for 20 minutes with 10% normal fetal calf serum in PBS followed by an one hour incubation with anti-VZV serum (1:1000). Wells were then rinsed with PBS and a secondary biotinylated goat anti-mouse antibody was added for 1 hour (Vector Laboratories, Burlingame, CA) followed by a streptavidin-alkaline phosphatase conjugate (Jackson ImmunoResearch, West Grove, PA) at a 1:500 dilution. Following a rinse in Tris-buffered saline (TBS), plates were developed using naphthol AS-MX phosphate/FAST RED substrate for 10 minutes. Red-stained plaques were counted using a dissection microscope (6X power) and photographed

using a Keyence BZ-X700 microscope. Plaque forming units (PFU)/mL were calculated and statistical analyses were performed using Student's t test Prism vers. 7.0C by GraphPad.

### Generation of rabbit monospecific antibody to VZV gM and immunoblot analysis of gM mutants.

A monospecific anti-gM antibody was produced against a keyhole limpet hemocyanin (KLH)-conjugated synthetic peptide [CEDELLYERSNGWE] (GenScript Corporation, Piscataway, NJ). Rabbits were bled after three immunizations with the KLH-peptide conjugate. Serum from a pre-immunization bleed was also obtained. The Ig fraction of the pre-immune serum and rabbit anti-gM serum were purified over an immobilized Protein A column (Pierce, Rockford, IL). Infected and uninfected cell lysates for immunoblot were harvested at 24 hours after infection in RIPA buffer (Boston Bio Products, Worcester, MA). Cell lysates were mixed with a glycerol-based loading dye and applied to 4–10% SDS-PAGE gradient gels. Following gel electrophoresis, protein was transferred to PVDF membranes (Millipore, Bedford, MA) and stained with amido black to ensure equal transfer of embedded protein. VZV antigens and cellular protein (α-tubulin) were detected using ECL reagents (Amersham, Buckinghamshire, England). Membrane-exposed film was imaged using a GS-710 instrument (Biorad, Hercules, CA) and analyzed using Quantity One software (Biorad). The rabbit polyclonal anti-IE63 and anti-gE antibodies were provided by Dr. Paul Kinchington.

### Plaque size determination.

For determination of plaque size, 24-well plates containing $1\times10^5$ MeWo cells/well were infected in triplicate with equivalent amounts of inoculum. At three days after infection, plaques were fixed and stained with FAST RED substrate. Stained plates were visualized and photographed under light microscopy (20X total magnification) and twenty plaques per virus were photographed using AxioControl software (AxioVision, version 3.1, Carl Zeiss Inc.). Individual JPEG images were imported into Image J and plaques were measured using the ruler function in the software program along a single vertical axis to determine the Feret diameter. Student's *t* test was performed to determine statistical significance using Prism version 7.0C by GraphPad.

### Immunofluorescent staining to determine gM localization.

VZV-infected cells were used to infect uninfected fibroblast monolayers ($1.5\times10^6$ cells/well) in 2-well chamber slides. At 48 hours post infection, cells were fixed and permeabilized with 2% paraformaldehyde containing 0.2% Triton-X 100 for 15 minutes at room temperature. Wells were washed twice with PBS and then blocked for 10 minutes with 10% goat serum in PBS. Mouse anti-gE antibody (EMD Millipore) and rabbit anti-gM were applied for 1 hour at room temperature. Secondary antibodies (Alexa Fluor 488 or Alexa Fluor 594, depending on species; Invitrogen) were applied for 1 hour at room temperature. Cells were washed 3 times for 10 minutes/wash between antibody applications. Cell nuclei were stained with Hoechst dye prior to viewing and imaging using a Zeiss LSM780 multiphoton laser scanning confocal microscope. Images were scanned at 1024×1024, 8-frame average, and a pinhole size of 1 airy unit. Control slides lacking application of the primary antibody were used in all staining experiments to establish background levels.

### Transmission electron microscopy (TEM).

Samples were processed for standard TEM. Briefly, infected MeWo cells on coverslips were fixed at 48 hours post by immersion in .05% gluteraldehyde/4% paraformaldehyde in 0.1M phosphate buffer. Samples were then post-fixed with osmium, dehydrated, infiltrated with EPON. After 24 hours to polymerize at 65°C, molds were thin sectioned with an ultramicrotome, sections were placed on copper grids, stained and viewed with a Phillips CM12 transmission electron microscope. The TEM protocol was optimized to visualize electron dense virion structures and enhance visibility of VZ-containing vacuoles. TEM images were photographed at magnifications from 5000 and 8300X, and cropped to highlight regions containing cell-free particles and particles within vacuoles. Since the standard TEM fixation method does not fully preserve morphology of membranous compartments, morphologic differences between rVOka and gM mutants cannot be determined.

### Experiments in SCID mice with skin and DRG xenografts.

The Stanford University Administrative Panel on Laboratory Animal Care reviewed and approved all animal protocols. All animal protocols complied with the Animal Welfare Act. Human tissues were obtained in accordance with state and federal regulations, and provided by Advanced Bioscience Resources (ABR, Alameda; CA). Generation and inoculation of severe compromised immunodeficient (SCID) mice with human skin and DRG xenografts has been previously described (27). Briefly, young male homozygous C.B.−17 *scid/scid* mice were implanted with full-thickness human skin xenografts under the dorsal rump or a single dorsal root ganglion under the renal capsule. After allowing for engraftment (four weeks for skin xenografts and 16 weeks for DRG xenograft), the mice were anesthetized and the exposed xenografts were inoculated with mutant viruses (approximately 50 μl/implant) in HELF cells by direct injection (DRG) or scarification (skin). For skin, mice were sedated and the implants were removed at 11 and 21 days after infection. One half of each implant was fixed in 4% paraformaldehyde for histological analysis, the remaining half was minced to a fine paste in PBS for titration of infectious virus. For DRG, xenografts were removed at 21 days after infection. The entire implant was fixed for histological analysis.

### VZV histopathology and immunostaining.

Ten micron paraffin sections from skin xenografts were dewaxed and rehydrated for immunohistochemical analysis. Slides were pretreated with 3% hydrogen peroxide and blocked for 10 minutes with blocking reagent (Chemicon International Inc., Temecula, CA). Rabbit anti-IE63, Ig fraction, was applied to sections at 1:500 for one hour at room temperature. A secondary biotinylated anti-rabbit Ig antibody was applied for 20 minutes at room temperature. Slides were developed using peroxidase-based enzyme detection methods with diaminobenzidine (DAB) substrate and hematoxylin nuclear counterstain as specified by the Chemicon Immunohistochemistry Kit (Chemicon International Inc., Temecula, CA). Slides were examined and photographed using a light microscope (Axiovert 200, Carl Zeiss Inc.).

## ACKNOWLEDGMENTS

The authors acknowledge Xibing Che and Susan Canny for their contributions to this project. The authors thank Mike Reichelt, Jaya Rajamani, Preeti Sikka and Michelle Lai for technical assistance. This work was supported by grants from The National Cancer Institute (CA049605) and the National Institute of Allergy and Infectious Diseases (AI053846 and AI20459)

## REFERENCES

1. Arvin AM, Moffat JF, Sommer M, Oliver S, Che X, Vleck S, Zerboni L, Ku CC. 2010 Varicella-zoster virus T cell tropism and the pathogenesis of skin infection. Curr Top Microbiol Immunol 342:189–209. [PubMed: 20397071]
2. Arvin AM, Gilden D. 2013 Varicella-Zoster Virus, p pp. 2015–2184 DM K PM H (ed), Fields Virology, 6th edition ed. Lippincott Williams & Wilkins, Philadelphia (Pennsylvania).
3. Wu SX, Zhu XP, Letchworth GJ. 1998 Bovine herpesvirus 1 glycoprotein forms a disulfide-linked heterodimer with the U(L)49.5 protein. J Virol 72:3029–36. [PubMed: 9525625]
4. Baines JD, Wills E, Jacob RJ, Pennington J, Roizman B. 2007 Glycoprotein M of herpes simplex virus 1 is incorporated into virions during budding at the inner nuclear membrane. J Virol 81:800–12. [PubMed: 17079321]
5. Klupp BG, Nixdorf R, Mettenleiter TC. 2000 Pseudorabies virus glycoprotein inhibits membrane fusion. J Virol 74:6760–8. [PubMed: 10888614]
6. Konig P, Giesow K, Keil GM. 2002 Glycoprotein M of bovine herpesvirus 1 (BHV-1) is nonessential for replication in cell culture and is involved in inhibition of bovine respiratory syncytial virus F protein induced syncytium formation in recombinant BHV-1 infected cells. Vet Microbiol 86:37–49. [PubMed: 11888688]
7. Yamagishi Y, Sadoaka T, Yoshii H, Somboonthum P, Imazawa T, Nagaike K, Ozono K, Yamanishi K, Mori Y. 2007 Varicella-zoster virus glycoprotein M is glycosylated, expressed on the viral envelope, and functions in viral cell-to-cell spread. Journal of Virology.
8. Sadaoka T, Yanagi T, Yamanishi K, Mori Y. 2010 Characterization of the varicella-zoster virus ORF50 gene, which encodes glycoprotein M. J Virol 84:3488–502. [PubMed: 20106918]
9. Letourneur F, Klausner RD. 1992 A novel di-leucine motif and a tyrosine-based motif independently mediate lysosomal targeting and endocytosis of CD3 chains. Cell 69:1143–57. [PubMed: 1535555]
10. Trowbridge IS, Collawn JF, Hopkins CR. 1993 Signal-dependent membrane protein trafficking in the endocytic pathway. Annu Rev Cell Biol 9:129–61. [PubMed: 8280459]
11. Dinkel H, Michael S, Weatheritt RJ, Davey NE, Van Roey K, Altenberg B, Toedt G, Uyar B, Seiler M, Budd A, Jodicke L, Dammert MA, Schroeter C, Hammer M, Schmidt T, Jehl P, McGuigan C, Dymecka M, Chica C, Luck K, Via A, Chatr-Aryamontri A, Haslam N, Grebnev G, Edwards RJ, Steinmetz MO, Meiselbach H, Diella F, Gibson TJ. 2012 ELM--the database of eukaryotic linear motifs. Nucleic Acids Res 40:D242–51. [PubMed: 22110040]
12. Pandey KN. 2009 Functional roles of short sequence motifs in the endocytosis of membrane receptors. Front Biosci (Landmark Ed) 14:5339–60. [PubMed: 19482617]
13. Kelly BT, McCoy AJ, Spate K, Miller SE, Evans PR, Honing S, Owen DJ. 2008 A structural explanation for the binding of endocytic dileucine motifs by the AP2 complex. Nature 456:976–79. [PubMed: 19140243]
14. Pasieka TJ, Maresova L, Grose C. 2003 A functional YNKI motif in the short cytoplasmic tail of varicella-zoster virus glycoprotein gH mediates clathrin-dependent and antibody-independent endocytosis. J Virol 77:4191–204. [PubMed: 12634377]
15. Heineman TC, Krudwig N, Hall SL. 2000 Cytoplasmic domain signal sequences that mediate transport of varicella-zoster virus gB from the endoplasmic reticulum to the Golgi. J Virol 74:9421–30. [PubMed: 11000211]
16. Olson JK, Grose C. 1997 Endocytosis and recycling of varicella-zoster virus Fc receptor glycoprotein gE: internalization mediated by a YXXL motif in the cytoplasmic tail. J Virol 71:4042–54. [PubMed: 9094682]

17. Cai JS, Jang HK, Izumiya Y, Tsushima Y, Kato K, Damiani AM, Miyazawa T, Kai C, Takahashi E, Mikami T. 1999 Identification and structure of the Marek's disease virus serotype 2 glycoprotein M gene: comparison with glycoprotein M genes of Herpesviridae family. J Vet Med Sci 61:503–11. [PubMed: 10379942]
18. Favoreel HW. 2006 The why's of Y-based motifs in alphaherpesvirus envelope proteins. Virus Res 117:202–8. [PubMed: 16417939]
19. Gershon AA, Sherman DL, Zhu Z, Gabel CA, Ambron RT, Gershon MD. 1994 Intracellular transport of newly synthesized varicella-zoster virus: final envelopment in the trans-Golgi network. J Virol 68:6372–90. [PubMed: 8083976]
20. Crump CM, Bruun B, Bell S, Pomeranz LE, Minson T, Browne HM. 2004 Alphaherpesvirus glycoprotein M causes the relocalization of plasma membrane proteins. J Gen Virol 85:3517–27. [PubMed: 15557225]
21. Nixdorf R, Klupp BG, Mettenleiter TC. 2001 Role of the cytoplasmic tails of pseudorabies virus glycoproteins B, E and M in intracellular localization and virion incorporation. J Gen Virol 82:215–26. [PubMed: 11125174]
22. Moffat J, Mo C, Cheng JJ, Sommer M, Zerboni L, Stamatis S, Arvin AM. 2004 Functions of the C-terminal domain of varicella-zoster virus glycoprotein E in viral replication in vitro and skin and T-cell tropism in vivo. J Virol 78:12406–15. [PubMed: 15507627]
23. Johnson DC, Webb M, Wisner TW, Brunetti C. 2001 Herpes simplex virus gE/gI sorts nascent virions to epithelial cell junctions, promoting virus spread. J Virol 75:821–33. [PubMed: 11134295]
24. Tomishima MJ, Smith GA, Enquist LW. 2001 Sorting and transport of alpha herpesviruses in axons. Traffic 2:429–36. [PubMed: 11422937]
25. Zerboni L, Berarducci B, Rajamani J, Jones CD, Zehnder JL, Arvin A. 2011 Varicella-zoster virus glycoprotein E is a critical determinant of virulence in the SCID mouse-human model of neuropathogenesis. J Virol 85:98–111. [PubMed: 20962081]
26. Mori Y, Sadaoka T. 2010 Varicella-zoster virus glycoprotein M. Curr Top Microbiol Immunol 342:147–54. [PubMed: 20373090]
27. Zerboni L, Hinchliffe S, Sommer MH, Ito H, Besser J, Stamatis S, Cheng J, Distefano D, Kraiouchkine N, Shaw A, Arvin AM. 2005 Analysis of varicella zoster virus attenuation by evaluation of chimeric parent Oka/vaccine Oka recombinant viruses in skin xenografts in the SCIDhu mouse model. Virology 332:337–46. [PubMed: 15661165]
28. Oliver SL, Yang E, Arvin AM. 2016 Varicella-Zoster Virus Glycoproteins: Entry, Replication, and Pathogenesis. Curr Clin Microbiol Rep 3:204–215. [PubMed: 28367398]
29. Oliver SL, Yang E, Arvin AM. 2017 Dysregulated Glycoprotein B-Mediated Cell-Cell Fusion Disrupts Varicella-Zoster Virus and Host Gene Transcription during Infection. J Virol 91.
30. Yang E, Arvin AM, Oliver SL. 2017 The Glycoprotein B Cytoplasmic Domain Lysine Cluster Is Critical for Varicella-Zoster Virus Cell-Cell Fusion Regulation and Infection. J Virol 91.
31. Harson R, Grose C. 1995 Egress of varicella-zoster virus from the melanoma cell: a tropism for the melanocyte. J Virol 69:4994–5010. [PubMed: 7609070]
32. Reichelt M, Brady J, Arvin AM. 2009 The replication cycle of varicella-zoster virus: analysis of the kinetics of viral protein expression, genome synthesis, and virion assembly at the single-cell level. J Virol 83:3904–18. [PubMed: 19193797]
33. Wang ZH, Gershon MD, Lungu O, Zhu Z, Mallory S, Arvin AM, Gershon AA. 2001 Essential role played by the C-terminal domain of glycoprotein I in envelopment of varicella-zoster virus in the trans-Golgi network: interactions of glycoproteins with tegument. J Virol 75:323–40. [PubMed: 11119602]
34. Padilla JA, Nii S, Grose C. 2003 Imaging of the varicella zoster virion in the viral highways: comparison with herpes simplex viruses 1 and 2, cytomegalovirus, pseudorabies virus, and human herpes viruses 6 and 7. J Med Virol 70 Suppl 1:S103–10. [PubMed: 12627497]
35. Tyzzer EE. 1906 The Histology of the Skin Lesions in Varicella. J Med Res 14:361–392 7. [PubMed: 19971703]
36. Gershon MD, Gershon AA. 2010 VZV infection of keratinocytes: production of cell-free infectious virions in vivo. Curr Top Microbiol Immunol 342:173–88. [PubMed: 20225011]

37. Moffat J, Ito H, Sommer M, Taylor S, Arvin AM. 2002 Glycoprotein I of varicella-zoster virus is required for viral replication in skin and T cells. J Virol 76:8468–71. [PubMed: 12134050]

38. Berarducci B, Rajamani J, Reichelt M, Sommer M, Zerboni L, Arvin AM. 2009 Deletion of the first cysteine-rich region of the varicella-zoster virus glycoprotein E ectodomain abolishes the gE and gI interaction and differentially affects cell-cell spread and viral entry. J Virol 83:228–40. [PubMed: 18945783]

39. Esiri MM, Tomlinson AH. 1972 Herpes Zoster. Demonstration of virus in trigeminal nerve and ganglion by immunofluorescence and electron microscopy. J Neurol Sci 15:35–48. [PubMed: 4332851]

40. Reichelt M, Zerboni L, Arvin AM. 2008 Mechanisms of varicella-zoster virus neuropathogenesis in human dorsal root ganglia. J Virol 82:3971–83. [PubMed: 18256143]

41. Zerboni L, Reichelt M, Arvin A. 2010 Varicella-zoster virus neurotropism in SCID mouse-human dorsal root ganglia xenografts. Curr Top Microbiol Immunol 342:255–76. [PubMed: 20225014]

42. Zerboni L, Reichelt M, Jones CD, Zehnder JL, Ito H, Arvin AM. 2007 Aberrant infection and persistence of varicella-zoster virus in human dorsal root ganglia in vivo in the absence of glycoprotein I. Proc Natl Acad Sci U S A 104:14086–91. [PubMed: 17709745]

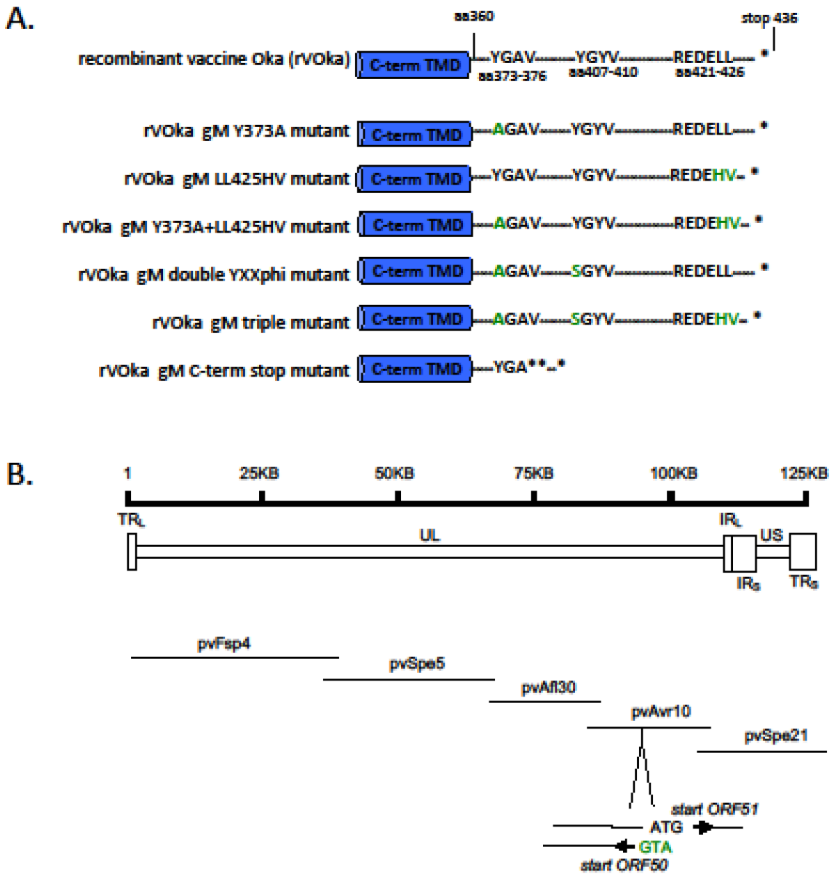


**Fig. 1. Construction of VZV gM mutants.**

**(A)** VZV gM has a 76 amino acid C-terminal domain (TMD) that contains two YXXΦ motifs, YGAV and YGYV (aa 373–376 and aa 407–410, respectively), and a dileucine (LL) motif within an acidic cluster (REDELL, aa 421 to 426) identified by linear motif scan. In all, six mutated pETVAVR fragments were generated using the recombinant vaccine Oka (rVOka) background. rVOka gM Y373A has a Y to A substitution in the YGAV sequence. rVOka gM LL425HV has a histidine-valine substituted for the native dileucines. rVOka gM Y373A+LL425HV has both of these changes. rVOka double YXXΦ has the Y373A change and a Y t o S substitution in the second YXXΦ motif. rVOka gM triple has all three changes: the Y373A, Y407S and LL425HV. The rVOka gM C-term stop mutant has two in-frame stop codons and one frame-shifted stop from aa 376. **(B)** The VZV genome is ~125 KB, and contains a unique long region (UL) flanked by repeats regions (long terminal repeat, $TR_L$, and long internal repeat $IR_L$) and a unique short region flanked by repeat regions (short internal repeat, $TR_S$, and short terminal repeat, $TR_S$). The VZV five cosmid system consists of five overlapping fragments of vaccine Oka strain cloned into SuperCos-1 cosmid vectors that recombine when cotransfected to form a single infectious clone of recombinant vaccine Oka strain (rVOka). ORF50 encodes VZV gM on the reverse strand of the 28506 basepair pvAvr10 cosmid at nucleotides 20198–18892. The start codons for ORF50 overlaps with the start codon for ORF51. ORF51 encodes the essential replication origin binding protein.

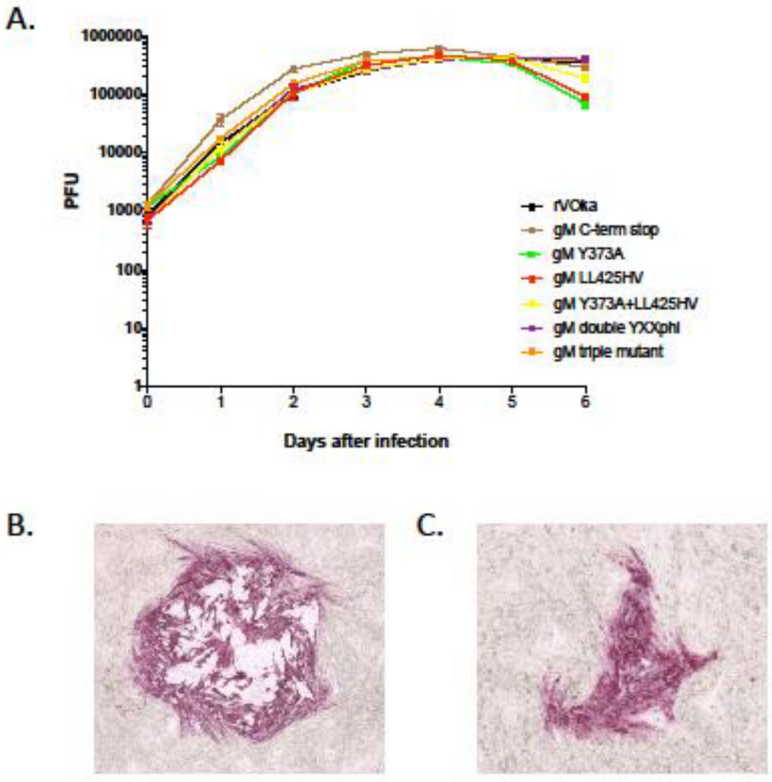


**Fig. 2. Replication kinetics of VZV gM C-terminal mutants.**

**(A)** The replication of VZV gM C-terminal mutants was evaluated by growth curve analysis in melanoma cells over a six day interval. The each data point represents the average of three replicate wells per timepoint. Error bars show standard error of mean. Color coding is as follows: rVOka (black), gM C-term stop (brown), gM Y373A (green), gM LL425HV (red), gM Y373A+LL425HV (yellow), gM double YXXΦ (purple), gM triple mutant (orange). **(B)** Representative plaque from rVOka-infected cells, immunostained using FastRed substrate. **(C)** Representative plaque from gM C-term stop-infected cells, immunostained using FastRed substrate.

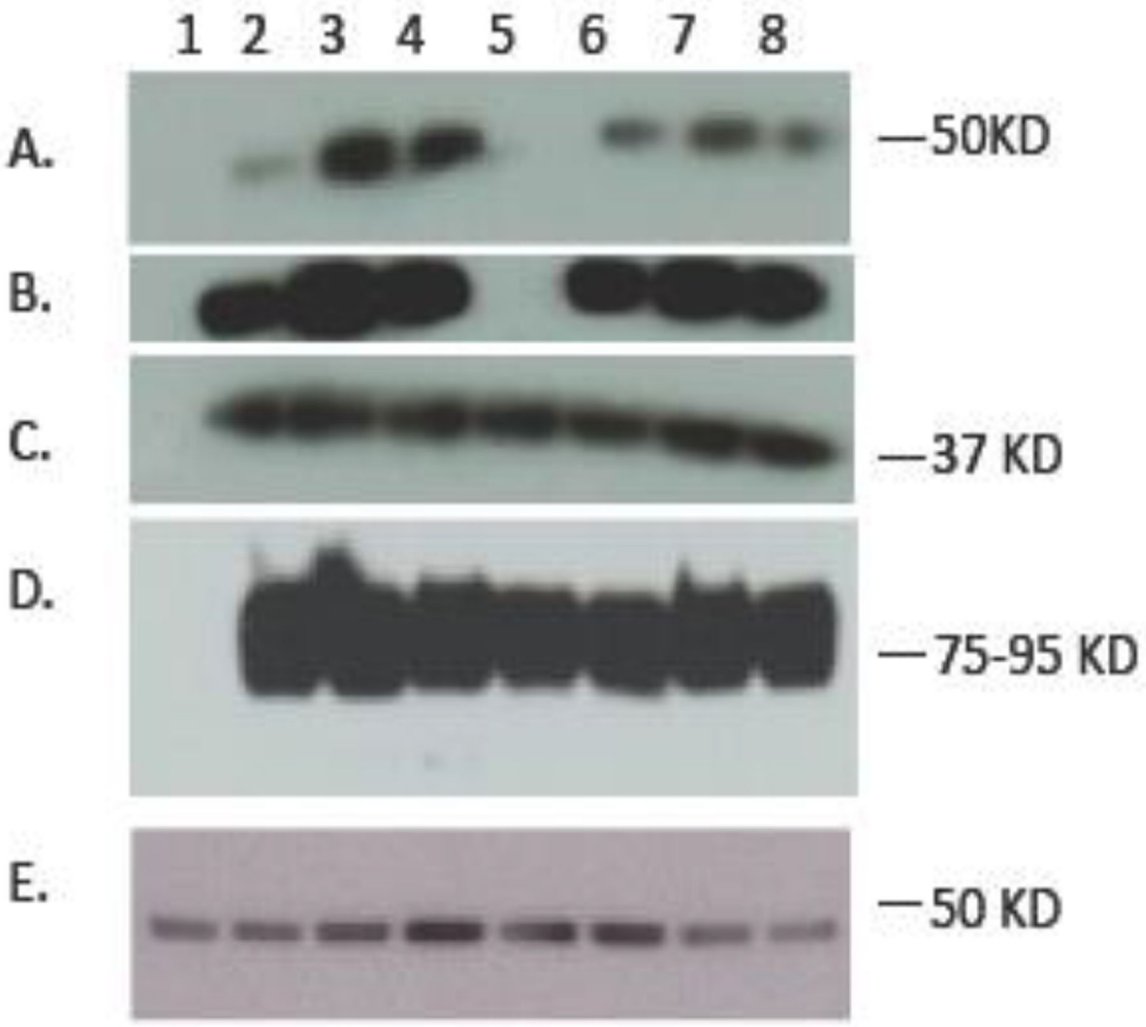


**Fig. 3. Immunoblot analysis of VZV gM C-terminal mutants.**

Infected cell lysates of VZV gM C-terminal mutants were run on a 4–20% SDS-PAGE gradient gel and probed using antibodies for (A) VZV gM, short exposure, (B) VZV gM, long exposure, (C) immediate early 63 protein, (D) VZV glycoprotein E and (E) cellular beta tubulin. Lanes are as follows: (1) uninfected MeWo cells, (2) rVOka, (3) gM triple mutant, (4) gM double YXXΦ, (5) gM C-term stop, (6) gM Y373A, (7) gM LL425HV, (8) gM Y373A+LL425HV. Expected approximate size of bands is shown in right in kilodaltons (KD).

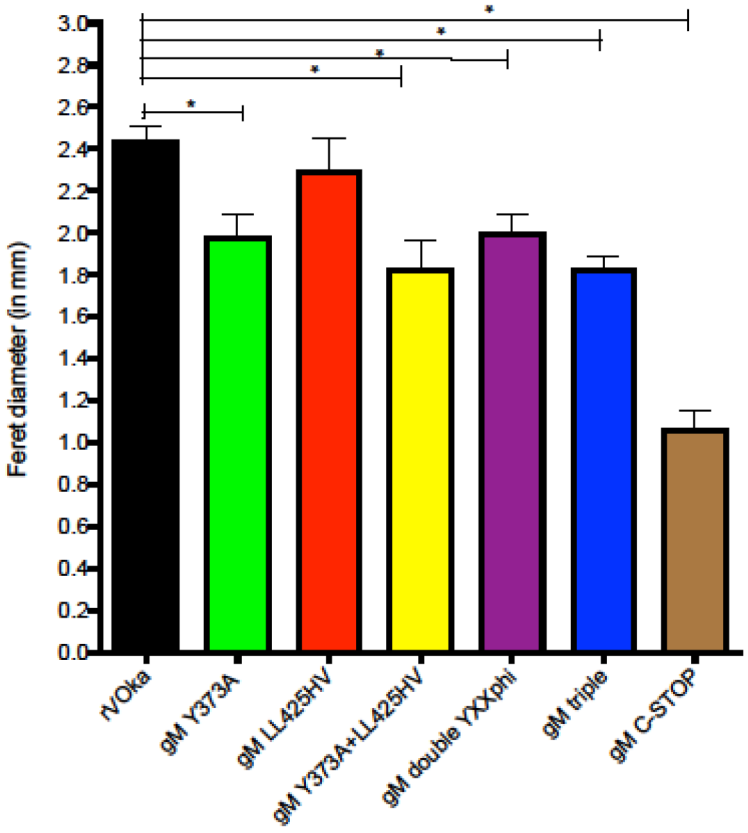


**Fig. 4. Comparison of plaque sizes.**

20–40 plaques/virus from titer plates at 48 hours after infection were visualized using a red precipitating substrate (FastRed) and photographed under light microscopy (20X total magnification) using AxioControl software (AxioVision, version 3.1, Carl Zeiss Inc). Individual JPEG images were imported into Image J and the Feret diameter (in mm) of each plaque was determined using the ruler function in the software program along a single vertical axis. Color coding is as follows: rVOka (black), gM C-term stop (brown), gM Y373A (green), gM LL425HV (red), gM Y373A+LL425HV (yellow), gM double YXXΦ (purple), gM triple mutant (orange). Student's *t* test was used to determine statistical significance; (*) <0.005).

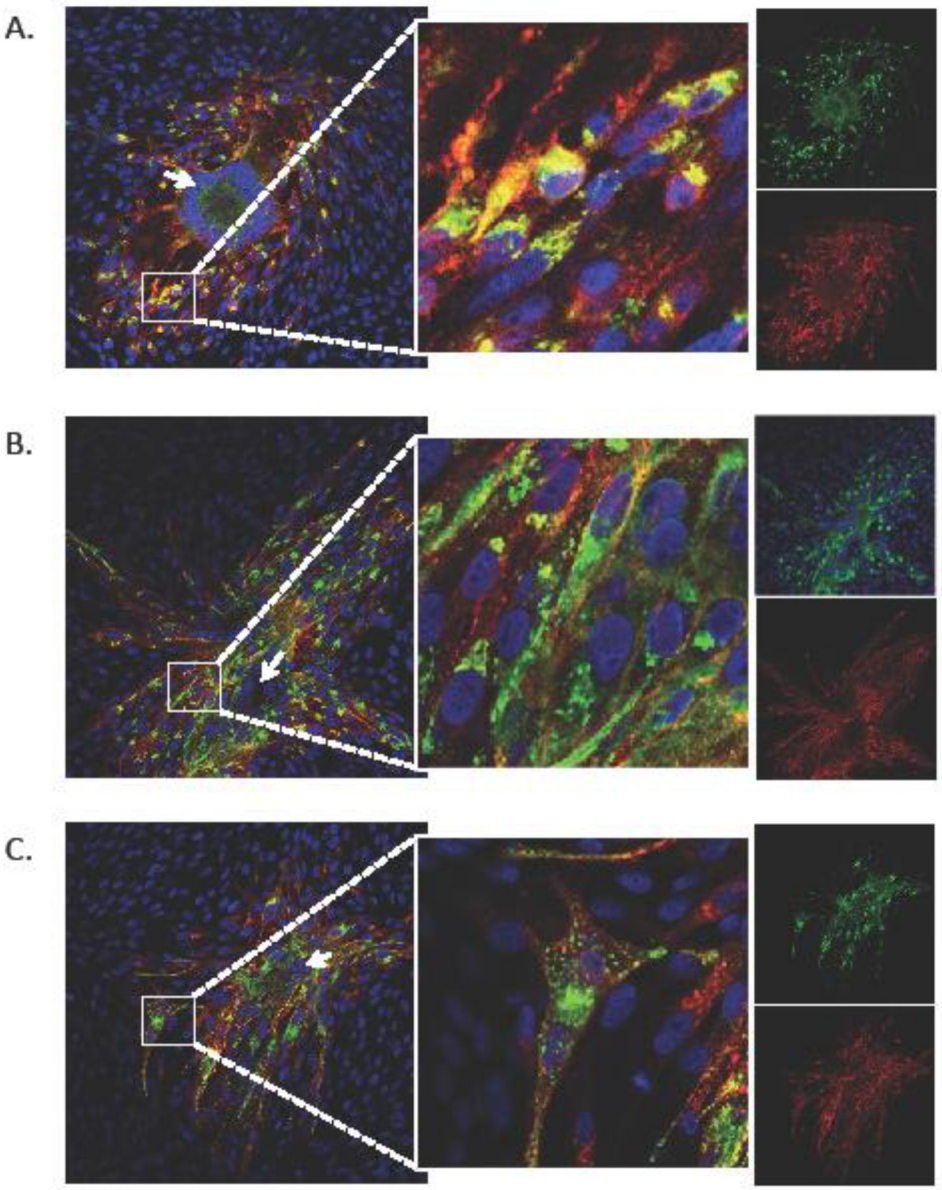


**Fig. 5. Localization of VZV gM in C-terminal mutants.**

The cellular localization of VZV gM in rVOka (A), the gM-double YxxΦ (B) and gM triple mutant (C) viruses was evaluated by confocal immunofluorescence of VZV-infected fibroblasts at 48 hours post infection using an anti-gE (red signal) and rabbit anti-gM (green signal). Cell nuclei are stained using Hoechst (blue). Inset panel (middle) shows high mag of small white square in left panel. Single color images for red and green signal are shown in the far right side. Arrows are described in Results.

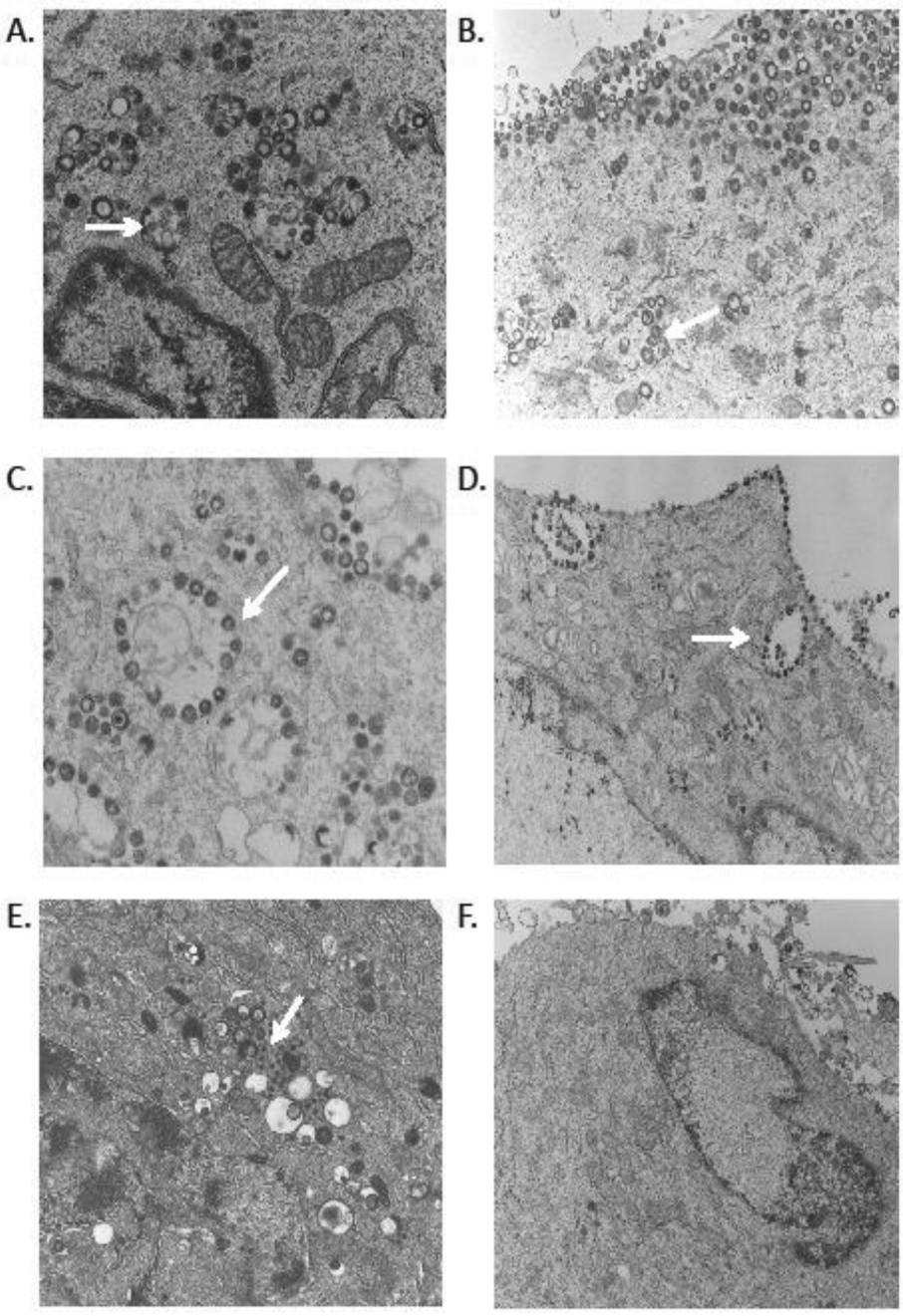


**Fig. 6. Transmission electron microscopy of VZV gM mutants in melanoma cells in vitro.**

VZV gM mutants were examined by TEM at 3 days post infection; (A) rVOka-infected MeWo cells, (B) gM Y373A mutant, (C) gM LL425HV mutant, (D) gM Y373A+LL425HV mutant, (E and F), gM C-term stop mutant. Magnification 5000–8300X.

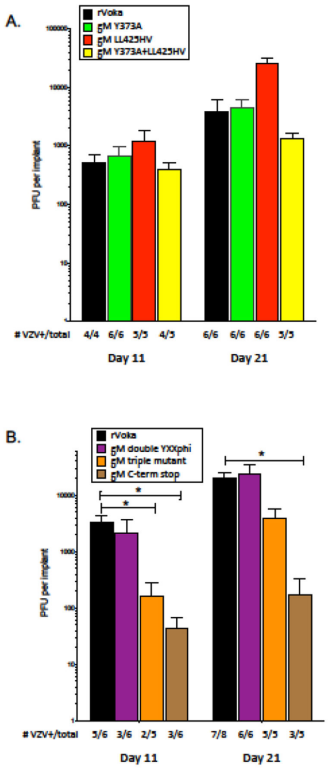


**Fig. 7. Replication of VZV gM C-terminal mutants in skin xenografts in SCID mice.**

Replication of VZV gM mutants was assessed in human skin xenografts in two separate experiments (A and B). Skin xenografts were inoculated by scarification with 50 ¼l/implant cell-associated VZV at $10^5$ PFU/mL. Infected skin xenografts were harvested at 11 and 21 days after inocualation. Skin homogenates were titered onto MeWo cells and stained 3 days later. Color coding is as follows: rVOka (black), gM C-term stop (brown), gM Y373A (green), gM LL425HV (red), gM Y373A+LL425HV (yellow), gM double YXXphi (purple), gM triple mutant (orange). At the bottom of each graph, the number of VZV-positive xenografts and total number inoculated are shown. (*) indicates $p<0.05$ by Student's t test.

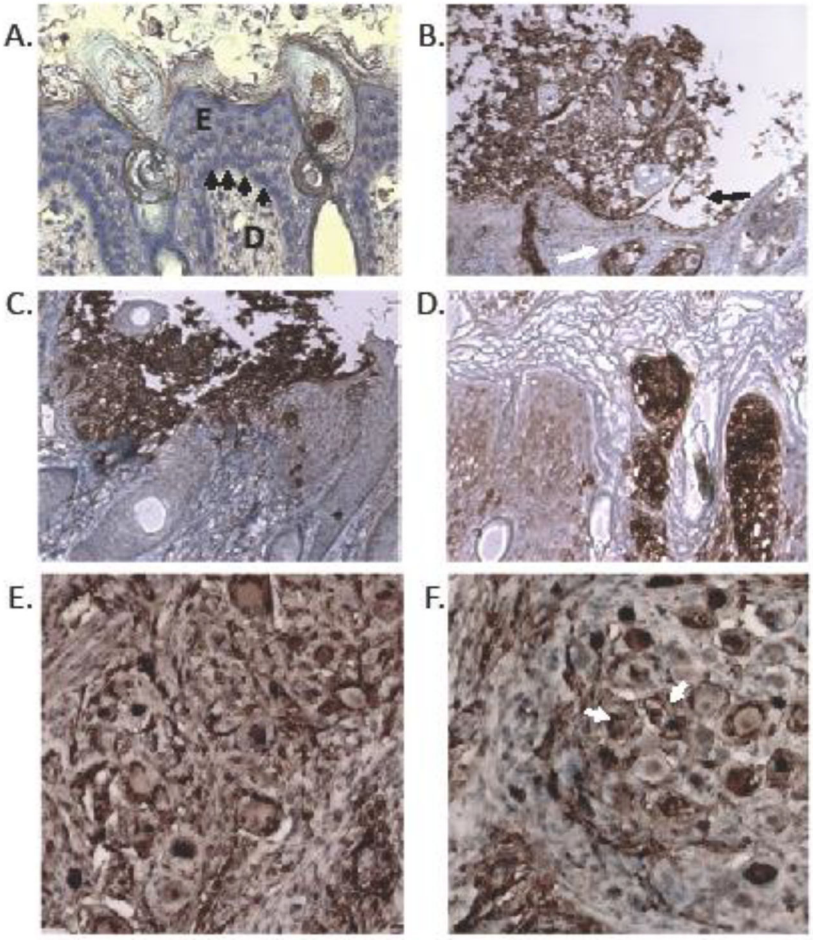


**Fig. 8. Histopathology of VZV gM mutants in skin and DRG xenografts in SCID mice.**

At 21 days post infection, sections of infected human skin xenografts were stained with antibody to VZV IE63 protein (brown, DAB substrate) and counterstained with hematoxylin (blue nuclear stain). Panels are as follows: (A) uninfected skin, (B) rVOka-infected skin, (C) gM triple mutant, (D) gM C-term mutant. At 21 days after infection, sections of rVOka (E) and gM C-STOP (F) human DRG xenografts were stained with antibody to VZV IE63 protein (brown, DAB substrate) and counterstained with hematoxylin (blue nuclear stain). Brown VZV-immunoreactive staining was apparent in neuronal cell bodies (white arrow) and encapsulating satellite glial cells.